

Supporting Information

Single Crystal Growth of Coordination Networks via Gas Phase and Crystal Size Dependence of Iodine Encapsulation

Tatsuhiko Kojima,[†] Wanuk Choi,[†] and Masaki Kawano*,[†]

*[†]Division of Advanced Materials Science, Pohang University of Science and Technology (POSTECH),
RIST Building 3-3390, 77 Cheongam-Ro, Nam-Gu, Pohang, Gyeongbuk, 790-784, Korea*

mkawano@postech.ac.kr

Contents pages

Experimental Details S3-S6

- Fig S1.** Photographs of time-dependent reaction and single crystals of each phase. S7
- Fig S2.** Overlay plot of the observed and simulated XRPD patterns of single crystals of **1**. S8
- Fig S3.** Overlay plot of the observed and simulated XRPD patterns of single crystals of **2**. S9
- Fig S4.** Overlay plot of the observed and simulated XRPD patterns of single crystals of **3**. S10
- Fig S5.** Overlay plot of the observed and simulated XRPD patterns, showing temperature dependence of products obtained from 1:1 mole ratio of ZnI_2 :TPT. S11
- Fig S6.** Overlay plot of the observed and simulated XRPD patterns, showing temperature dependence of products obtained from 2:3 mole ratio of ZnI_2 :TPT. S12
- Fig S7.** Overlay plot of the observed and simulated XRPD patterns, showing temperature dependence of products obtained from 1:2 mole ratio of ZnI_2 :TPT. S13
- Fig S8.** Ellipsoidal models of asymmetric unit in **1**, **2** and **3**, and number of bond formation in asymmetric unit. S14
- Fig S9.** TG plots of single crystals of **1**, **2**, and **3**. S15
- Fig S10.** XRPD change of **1** by heating at 703 K. S16
- Fig S11.** Microscope images and face indexing of single crystals of **2**. S17
- Fig S12.** Scheme of crystal growth of **2** via gas phase. S17
- Fig S13.** Crystal structures of **2** and **2**·nitrobenzen. S18
- Fig S14.** Overlay plot of the observed and simulated XRPD patterns of **2**·nitrobenzen. S18
- Fig S15.** Scheme of nitrobenzene encapsulation from cut edge along channel direction, [001]. S19
- Fig S16.** Overlay plot of the observed XRPD patterns of I_2 encapsulation in microcrystalline powder and single crystals of **2**. S20
- Fig S17.** Overlay plot of the observed XRPD patterns of I_2 encapsulation in microcrystalline powder and single crystals of **2**. S20
- Fig S18.** SEM images of **2** and microscope images of **2** immersed in I_2 nitrobenzene solution without and with nitrobenzene treatment. S21
- Fig S19.** Scheme of capping the channel entrance by I_2 and nitrobenzene encapsulation. S22
- Fig S20.** Overlay plot of the observed XRPD patterns of nitrobenzene treatment and I_2 encapsulation in single crystals of **2**. S23
- Fig S21.** Microscope images of a single crystal of **2** with nitrobenzene treatment after exposure to I_2 vapor. S23
- Reference.** S24

General Experimental Details

Reagents and general procedures

All the chemicals were used without any further purification. TPT (TPT = 2,4,6-tris(4-pyridyl)triazine) was synthesized according to the procedure described in the literature (ref 1).

Powder X-ray diffraction data were collected on a Bruker D8 ADVANCE instrument in house ($\text{CuK}\alpha_1$, $\lambda=1.5406 \text{ \AA}$). Synchrotron PXRD pattern of the powder of **2** immersed in nitrobenzene was recorded in transmission mode [0.3 mm capillary; synchrotron radiation $\lambda = 0.99967 \text{ \AA}$; Blue-IP detector; 2θ range: $2\text{--}70^\circ$; step width: 0.02° ; data collection time: 15 min] on a diffractometer equipped with a blue imaging plate detector at SPring-8 BL19B2 beam line. FTIR-ATR (attenuated total reflection) spectra were recorded on a Varian 670-IR FT-IR spectrometer ($650\text{--}4000 \text{ cm}^{-1}$). Thermogravimetric (TG) analysis was carried out at a ramp rate of 10 K/min in a nitrogen flow (20 ml/min) with Scinco TGA N-1000. Elemental analyses were performed by Vario MICRO Cube (Elementar) at Technical Support Center in Pohang University of Science and Technology. SEM images were collected by Hitachi S-4800 at 3.0kV.

Single crystal X-ray structure determination

The diffraction data for **1** was recorded with a RIGAKU/MSM Mercury CCD X-ray diffractometer with a synchrotron radiation ($\lambda = 0.6889 \text{ \AA}$) at PF-AR (NW2A beamline) of the High Energy Accelerator Research Organization (KEK). The diffraction images were processed by using HKL2000.² The diffraction data for **2** and **3** were recorded with an ADSC Q210 CCD area detector with a synchrotron radiation at 2D beamline in Pohang Accelerator Laboratory (PAL). The diffraction images were processed by using HKL3000.² Absorption correction for all data was performed with the program PLATON.³ Each structure was solved by the direct method of SHELXS-97 and refined by the full-matrix least-squares method on F^2 using SHLEXL-97.⁴

Synthesis

Preparation of **1** via gas phase.

TPT (3.1 mg, 0.01 mmol) and ZnI₂ (3.2 mg, 0.01 mmol) were uniformly mixed by a mortar and put into a glass ampule (10 ml). After evacuating inside (~ 0.1 Torr), the glass ampule was sealed. On rapidly heating it at 708 K and keeping the temperature for 2 hours, single crystals of **1** were formed inside of the glass ampule (yield: 92.1%). Found: C, 34.05; H, 1.83; N, 13.16. Calc. for C₁₈H₁₂I₂N₆Zn₁ {[ZnI₂](TPT)}: C, 34.23; H, 1.92; N, 13.31 %. IR (ATR, ν_{max}/cm⁻¹): 3050vw, 1620m, 1600m, 1580m, 1520vs, 1420w, 1370s, 1320m, 1240w, 1220m, 1210w, 1160w, 1100w, 1060m, 1020m, 995vw, 965vw, 890vw, 875w, 860w, 840w, 800s, 750w, 735w, 720vw, 700w, 670m, 660m.

Preparation of **2** via gas phase.

TPT (3.1 mg, 0.01 mmol) and ZnI₂ (4.8 mg, 0.015 mmol) were uniformly mixed by a mortar and put into a glass ampule (10 ml). After evacuating inside (~ 0.1 Torr), the glass ampule was sealed. On rapidly heating it at 743 K and keeping the temperature for 2 hours, single crystals of **2** were formed inside of the glass ampule (yield: 92.1%). Found: C, 27.41; H, 1.64; N, 10.69. Calc. for C₃₆H₂₄I₆N₁₂Zn₃ {[ZnI₂]₃(TPT)₂}: C, 27.33; H, 1.53; N, 10.62 %. IR (ATR, ν_{max}/cm⁻¹): 3050vw, 1620m, 1580m, 1520vs, 1490m, 1420w, 1380s, 1320m, 1235w, 1215m, 1100w, 1060m, 1020m, 990vw, 980vw, 890w, 875w, 860w, 840w, 800s, 750w, 740w, 700w, 670m, 650m.

Preparation of **3** via gas phase.

TPT (3.1 mg, 0.01 mmol) and ZnI_2 (6.4 mg, 0.02 mmol) were uniformly mixed by a mortar and put into a glass ampule (10 ml). After evacuating inside (~ 0.1 Torr), the glass ampule was sealed. On rapidly heating it at 843 K and keeping the temperature for 4 min, single crystals of **3** were formed inside of the glass ampule (yield: 56.4%). Found: C, 22.74; H, 1.27; N, 8.84. Calc. for $\text{C}_{18}\text{H}_{12}\text{I}_4\text{N}_6\text{Zn}_2 \{[(\text{ZnI}_2)_2(\text{TPT})]\}$: C, 22.83; H, 1.39; N, 8.74 %. IR (ATR, $\nu_{\text{max}}/\text{cm}^{-1}$): 3050vw, 1620m, 1570m, 1520vs, 1480m, 1420w, 1375s, 1315m, 1235w, 1210w, 1100w, 1060m, 1020m, 990vw, 970vw, 870w, 850w, 840w, 800s, 750w, 730w, 710w, 670m, 650m.

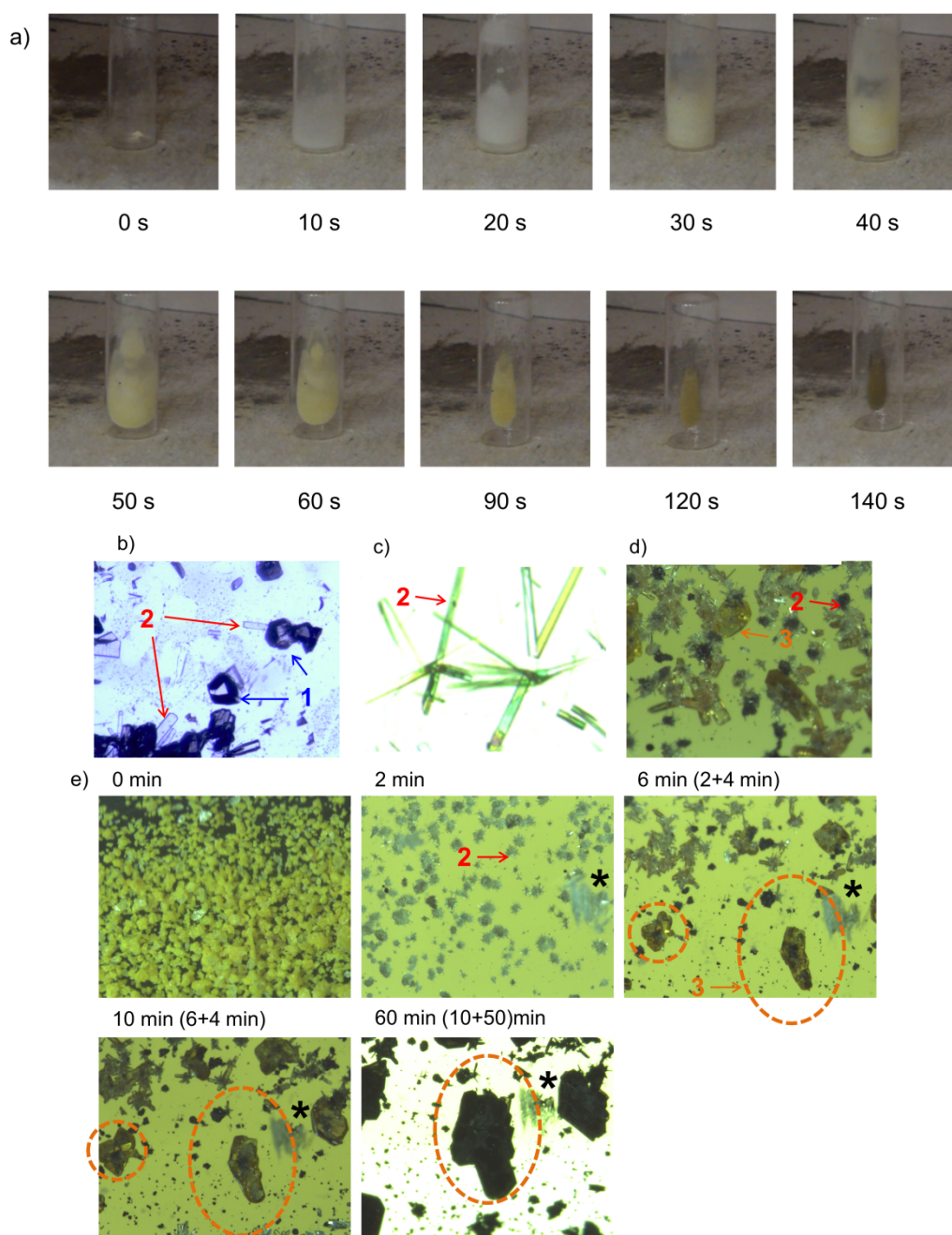


Fig S1. Photographs of time-dependent reaction and single crystals of each phase. a) time-dependent reaction of ZnI_2 and TPT (6 mg, at the mole ratio of 2:1, ~ 0.1 Torr, at 850 K). b) Mixture of single crystals of **1** and **2**. Single crystals of **2** grew on the surface of single crystals of **1**, indicating that **2** is more thermodynamic product than **1**. c) Single crystals of **2**. d) Mixture of single crystals of **2** (tiny plate) and **3** (block). e) Observation of time-dependent crystal growth of **3** at same position (repeat of heating at 800 K, 7.2 mg of ZnI_2 and TPT at 2:1mole ratio, ~ 0.25 Torr). Crystal size in orange dotted circle increased, indicating crystal growth via gas phase rather than solid-liquid interface. *: scratch as a scale.

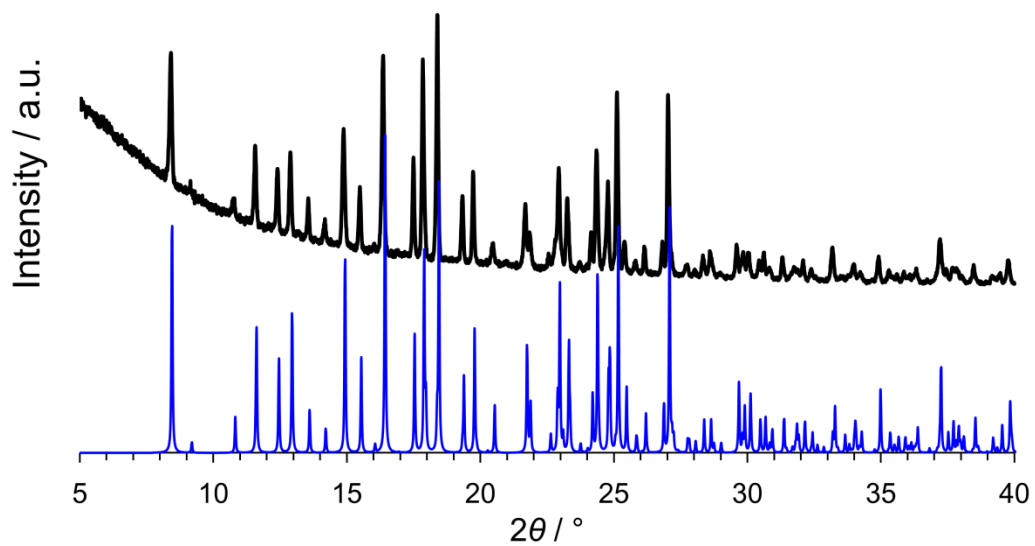


Fig S2. Overlay plot of the observed and simulated XRPD patterns of single crystals of **1**. Black: observed from the isolated single crystals of **1**. Blue: simulated from single crystal XRD data of **1**.

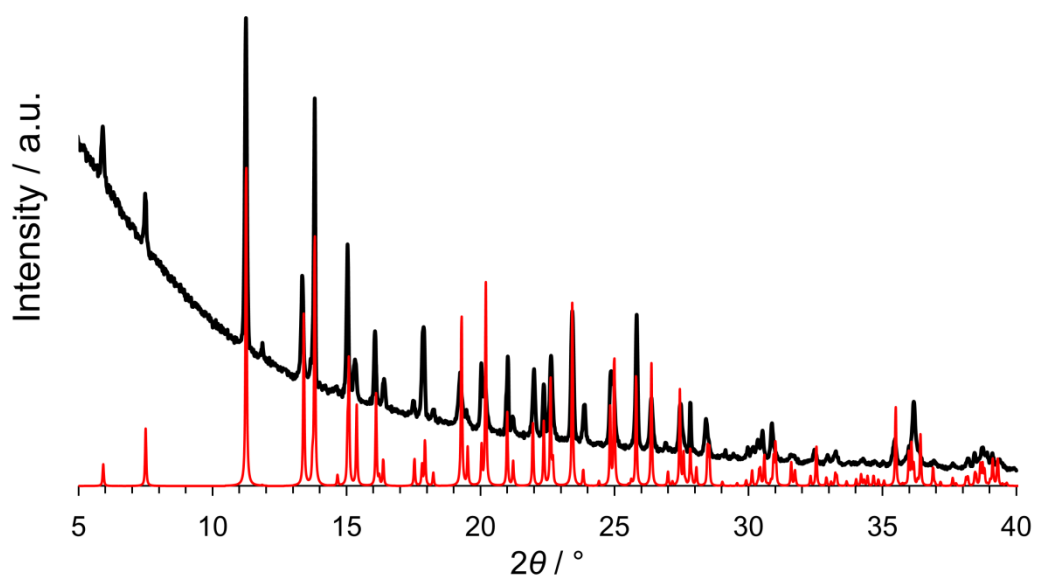


Fig S3. Overlay plot of the observed and simulated XRPD patterns of single crystals of **2**. Black: observed from the isolated single crystals of **2**. Red: simulated from single crystal XRD data of **2**.

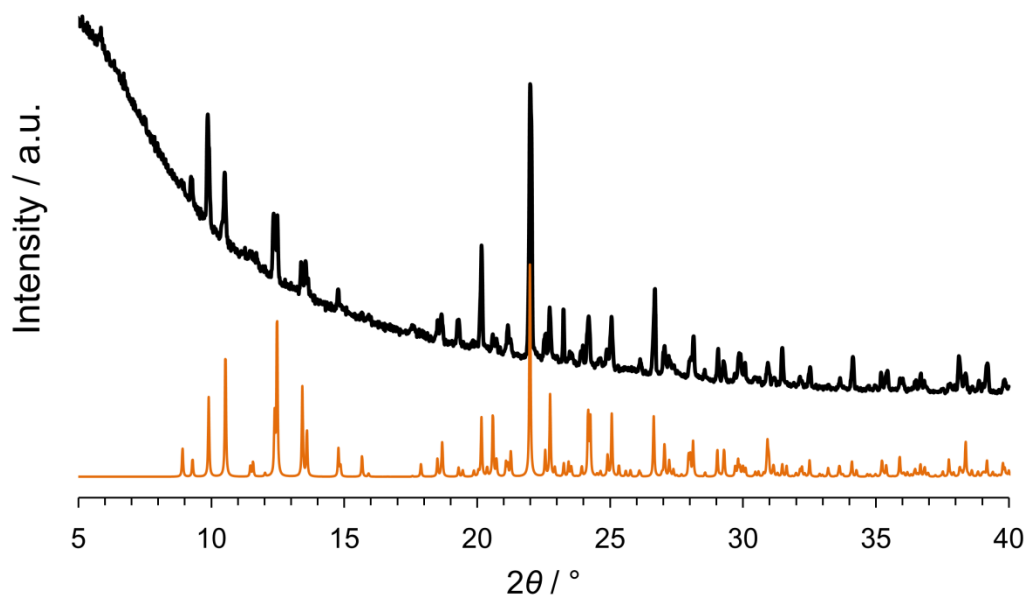


Fig S4. Overlay plot of the observed and simulated XRPD patterns of single crystals of **3**. Black: observed from the isolated single crystals of **3**. Orange: simulated from single crystal XRD data of **3**.

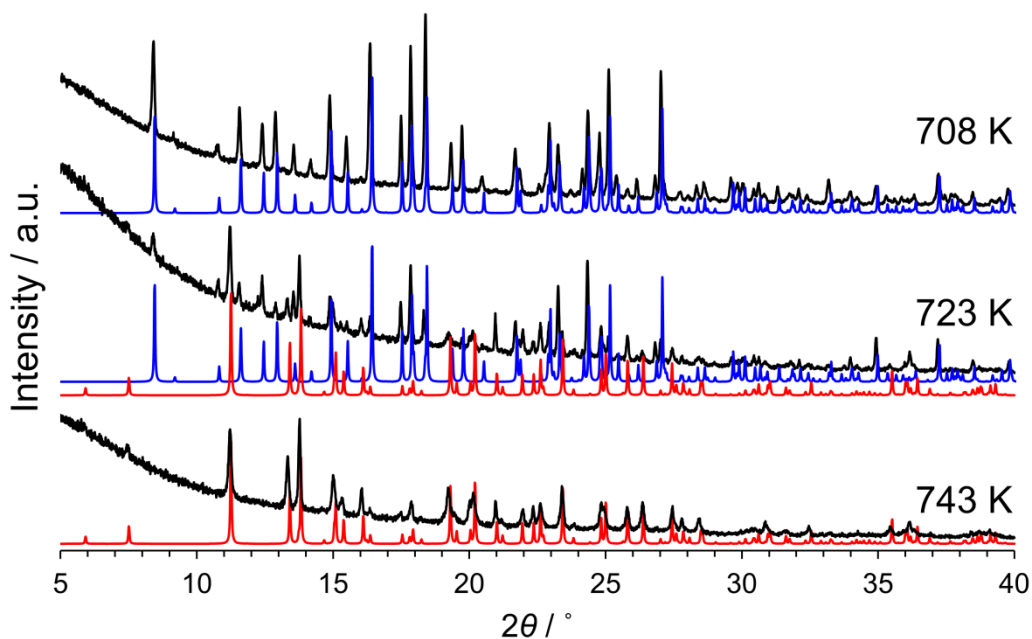


Fig S5. Overlay plot of the observed and simulated XRPD patterns, showing temperature dependence of products obtained from 1:1 mole ratio of ZnI_2 :TPT. Top) Black: observed from the single crystals obtained at 708 K. Blue: simulated from single crystal XRD data of **1**. Middle) Black: observed from the single crystals obtained at 723 K, includes two phases. Blue: simulated from single crystal XRD data of **1**. Red: simulated from single crystal XRD data of **2**. Bottom) Black: observed from the single crystals obtained at 743 K. Red: simulated from single crystal XRD data of **2**.

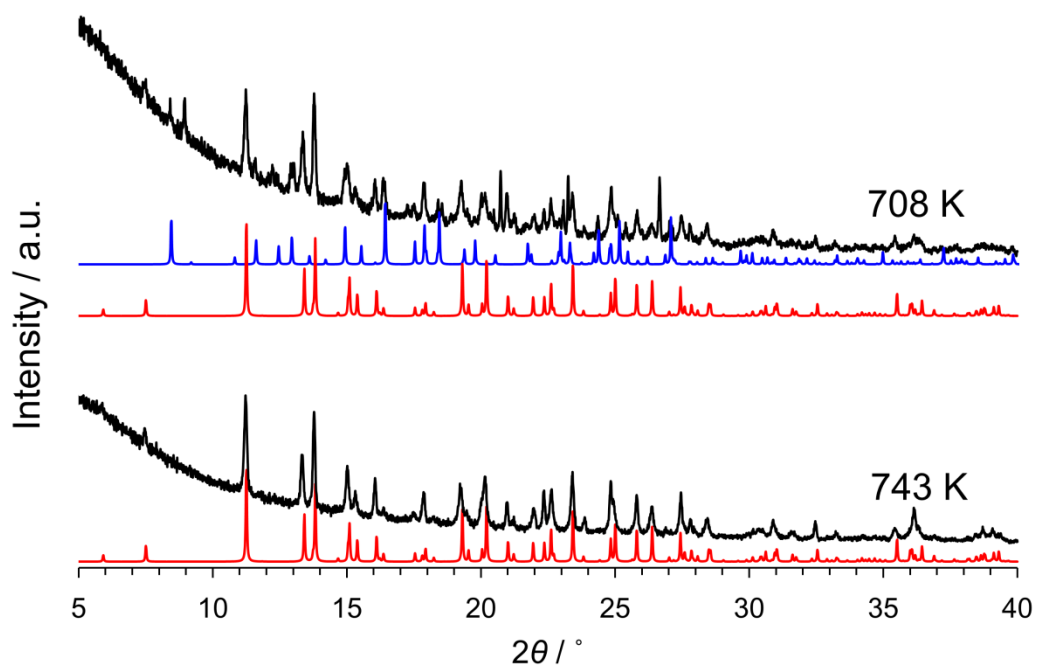


Fig S6. Overlay plot of the observed and simulated XRPD patterns, showing temperature dependence of products obtained from 2:3 mole ratio of ZnI_2 :TPT. Top) Black: observed from the single crystals obtained at 708 K, which includes two phases. Blue: simulated from single crystal XRD data of **1**. Red: simulated from single crystal XRD data of **2**. Bottom) Black: observed from the single crystals obtained at 743 K. Red: simulated from single crystal XRD data of **2**.

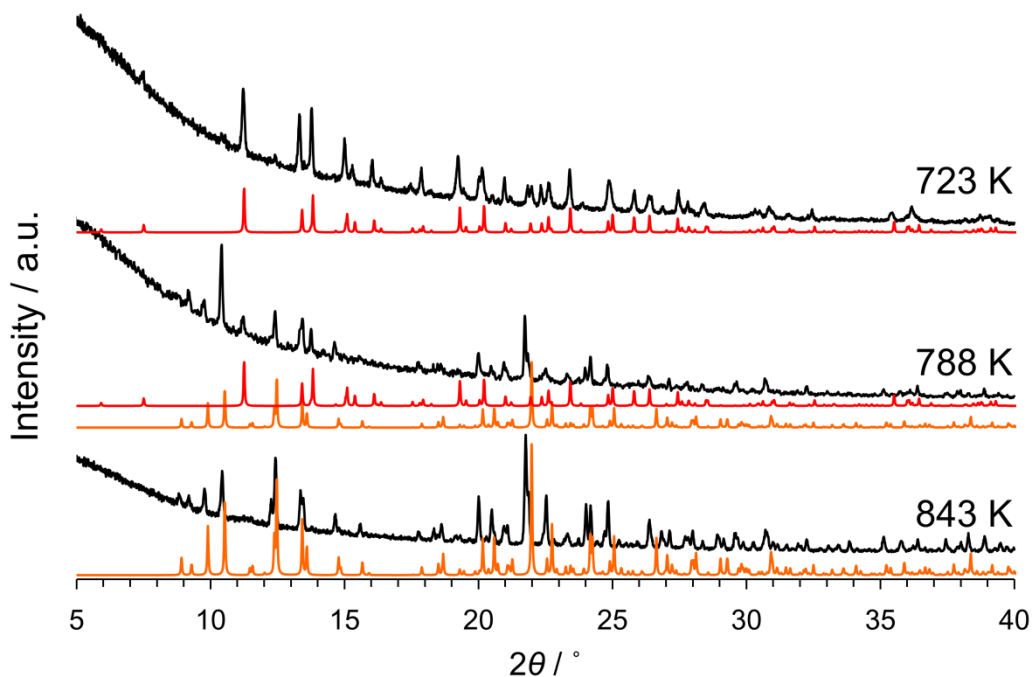


Fig S7. Overlay plot of the observed and simulated XRPD patterns, showing temperature dependence of products obtained from 1:2 mole ratio of ZnI_2 :TPT. Top) Black: observed from the single crystals obtained at 743 K. Red: simulated from single crystal XRD data of **2**. Middle) Black: observed from the single crystals obtained at 788 K, which includes two phases. Red: simulated from single crystal XRD data of **2**. Orange: simulated from single crystal XRD data of **3**. Bottom) Black: observed from the single crystals obtained at 843 K. Orange: simulated from single crystal XRD data of **3**.

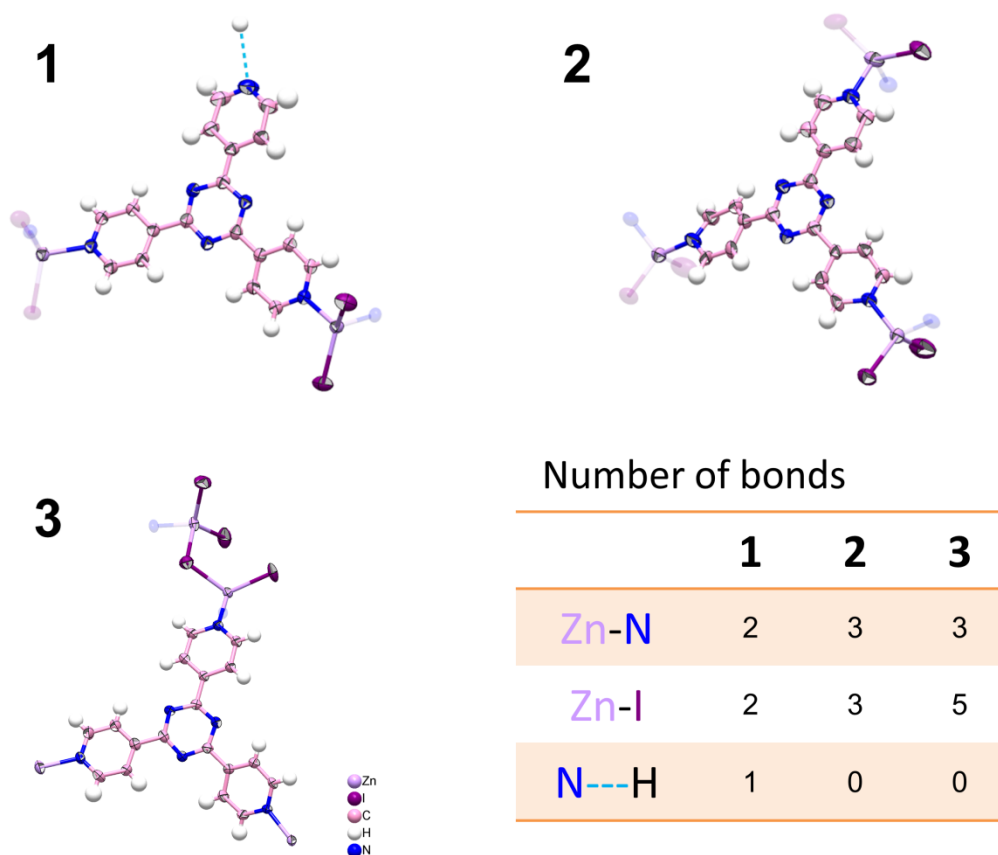


Fig S8. Ellipsoidal models of asymmetric unit in **1**, **2** and **3**, and number of bond formation (Zn-N, Zn-I, and N---H) in asymmetric unit. Displacement ellipsoids for non-H atoms are scaled to enclose 50% probability levels.

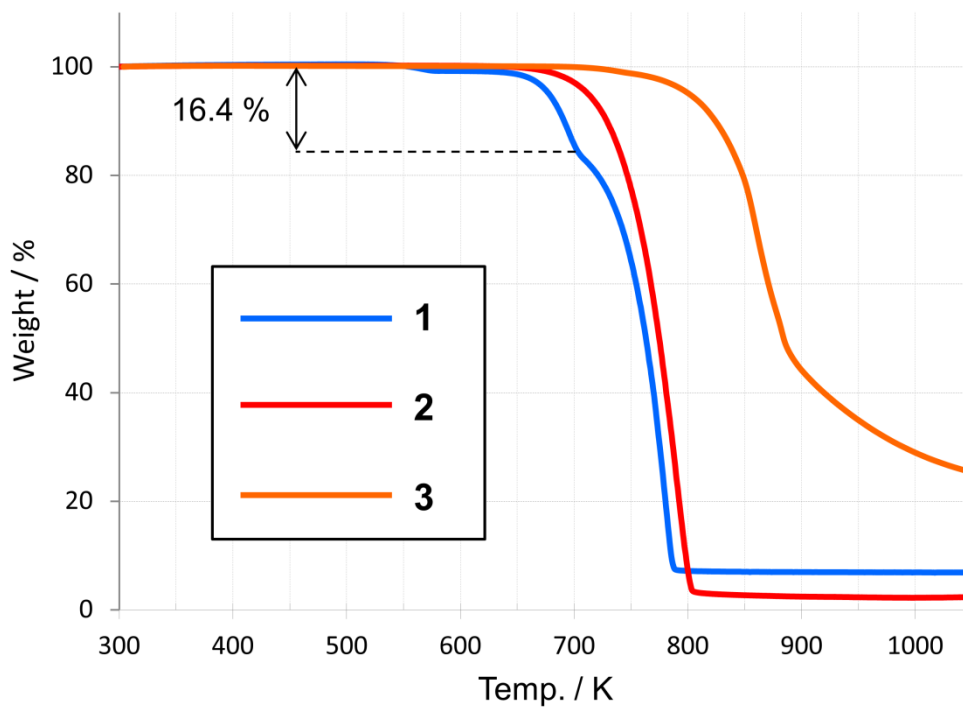


Fig S9. TG plots of single crystals of **1**, **2**, and **3**. Blue: **1**. Red: **2**. Orange: **3**. The first decrease of weight in **1** (16.4 %) corresponds to $\text{TPT} / 3 \times [(\text{ZnI}_2)(\text{TPT})] = 312.3 / 1894.6 = 0.165$, indicating removal of one TPT from $3 \times [(\text{ZnI}_2)(\text{TPT})]$ (ex. $3 \times [(\text{ZnI}_2)(\text{TPT})] \rightarrow [(\text{ZnI}_2)_3(\text{TPT})_2] + \text{TPT}$).

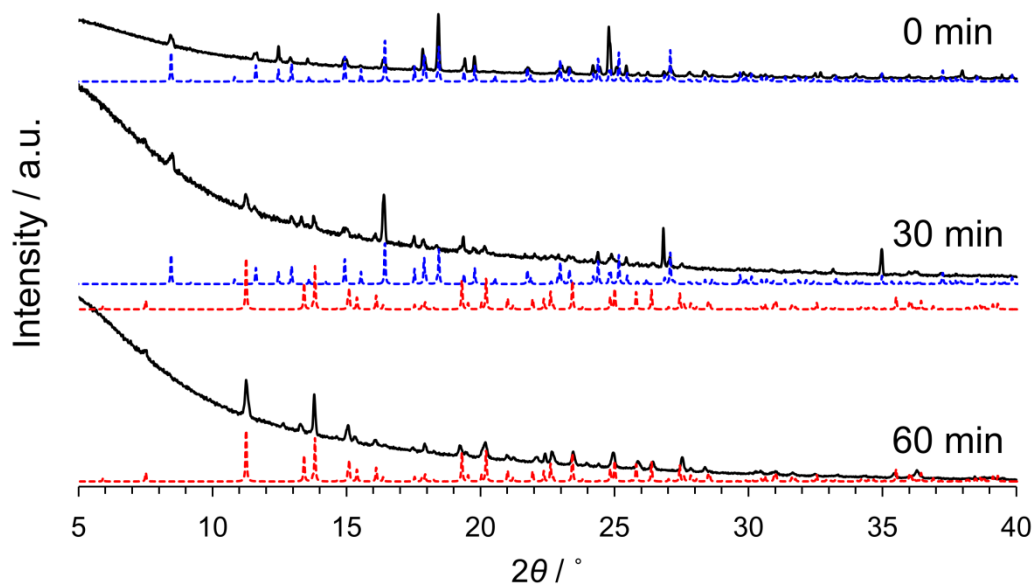


Fig S10. XRPD change of **1** by heating at 703 K, showing phase transition from **1** to **2**. Top) Black: observed from the single crystals of **1**. Blue: simulated from single crystal XRD data of **1**. Middle) Black: observed from the single crystals after heating **1** at 703 K for 30 min. Blue: simulated from single crystal XRD data of **1**. Red: simulated from single crystal XRD data of **2**. c) Black: observed from the single crystals after heating **1** at 703 K for 60 min. Red: simulated from single crystal XRD data of **2**.

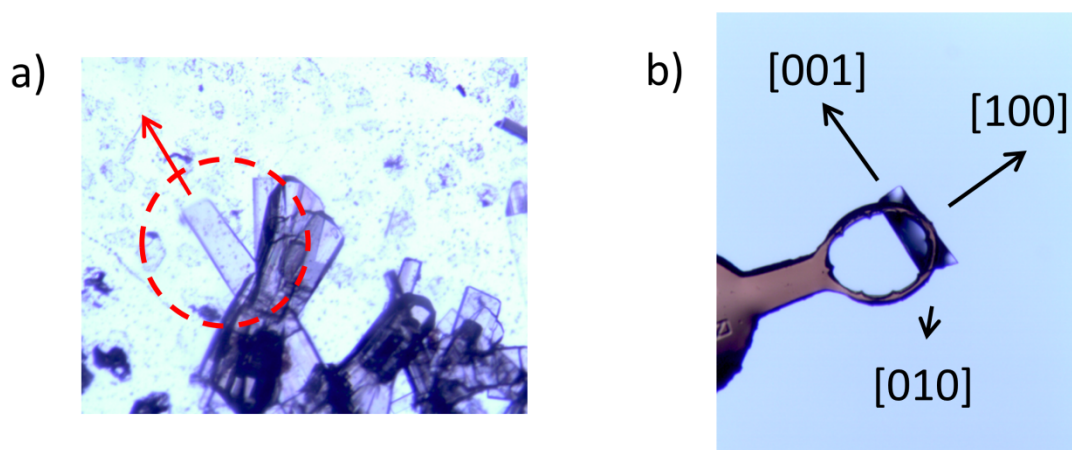


Fig S11. Microscope images and face indexing of single crystals of **2**. a) Crystal growth of **2** via gas phase in the direction to red arrow. b) Face indexing of single crystal of **2**. The direction of crystal growth via gas phase is [001].

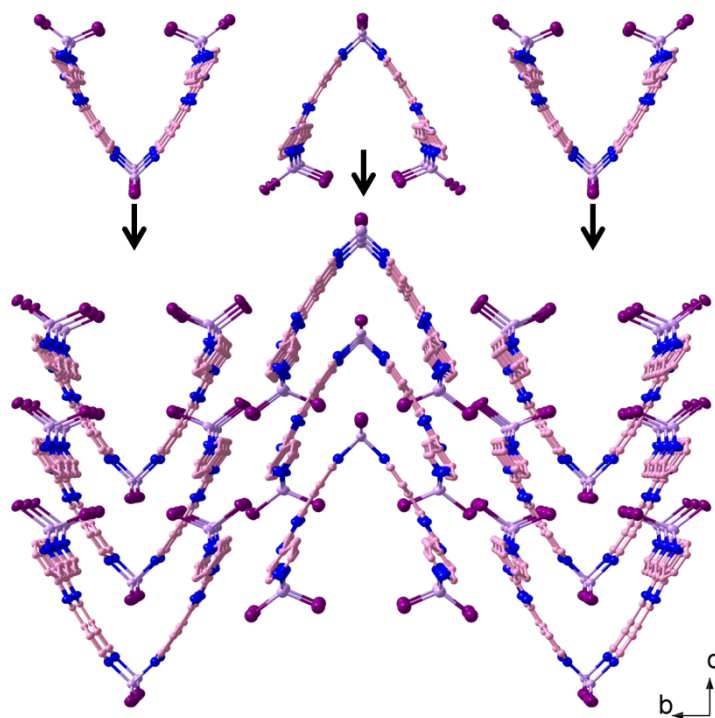


Fig S12. Scheme of crystal growth of **2** via gas phase along the [001] direction which corresponds to pore channel. Stacking of one dimensional saddle units via π - π interaction.

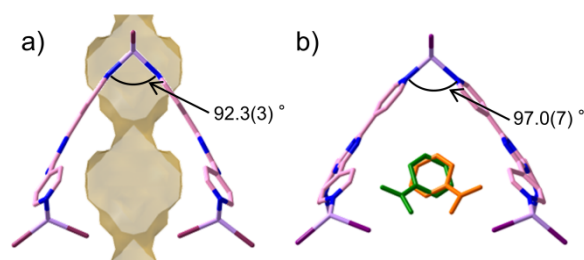


Fig S13. Crystal structures of **2** and **2**-nitrobenzene. a) 1D channel of pore in **2**. b) Symmetrically disordered nitrobenzene with site occupancy factor 0.5/0.5 in **2**-nitrobenzene. The angle of N-Zn-N in saddle unit increased from $92.3(3)^\circ$ to $97.0(7)^\circ$ in **2**-nitrobenzene and the void space increased from 147 \AA^3 to 262 \AA^3 (Calculated on PLATON).³

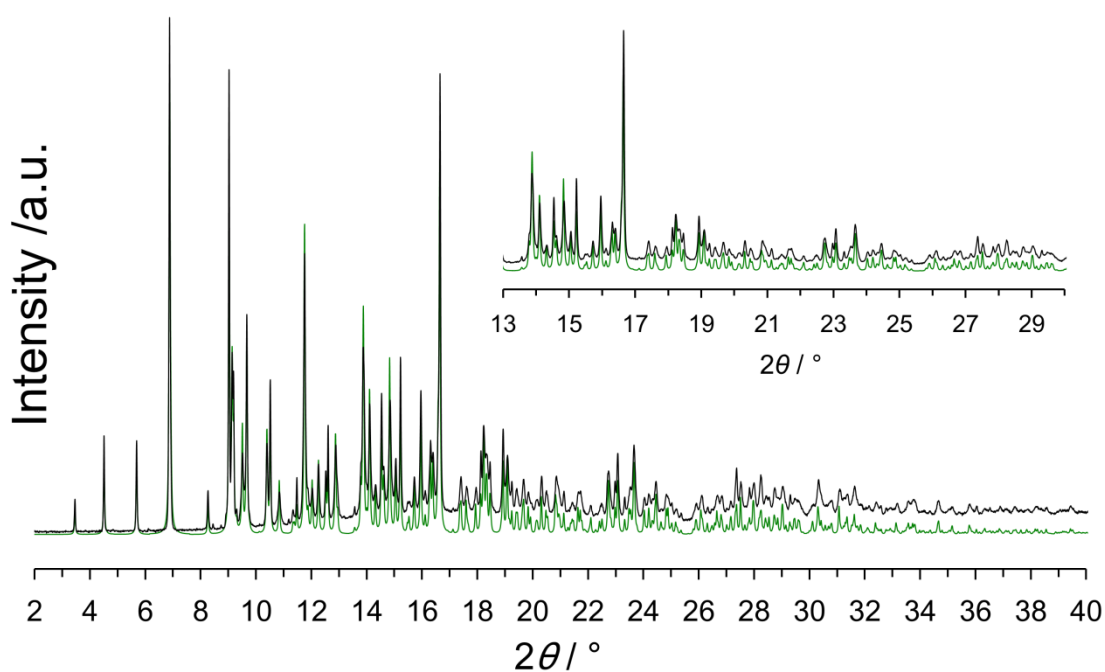


Fig S14. Overlay plot of the observed and simulated XRPD patterns of **2**-nitrobenzene. Black: Synchrotron PXRD pattern of the powder of **2** immersed in nitrobenzene. The data was collected at SPring-8 BL19B2 beam line ($\lambda = 0.99967 \text{ \AA}$, at R.T.). Green: simulated from single crystal XRD data of **2**-nitrobenzene. Inset shows magnified XRPD patterns.

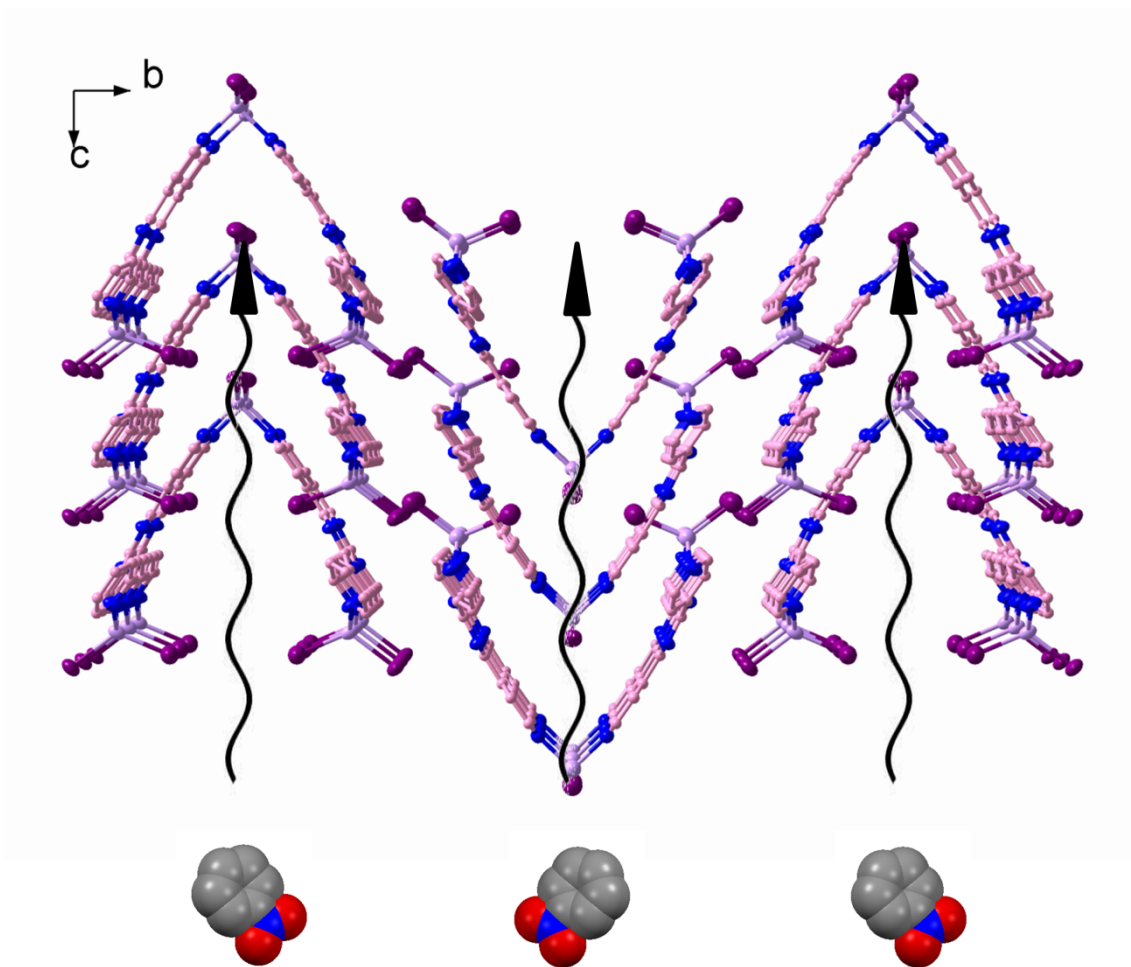


Fig S15. Scheme of nitrobenzene encapsulation from cut edge along channel direction, $[001]$.

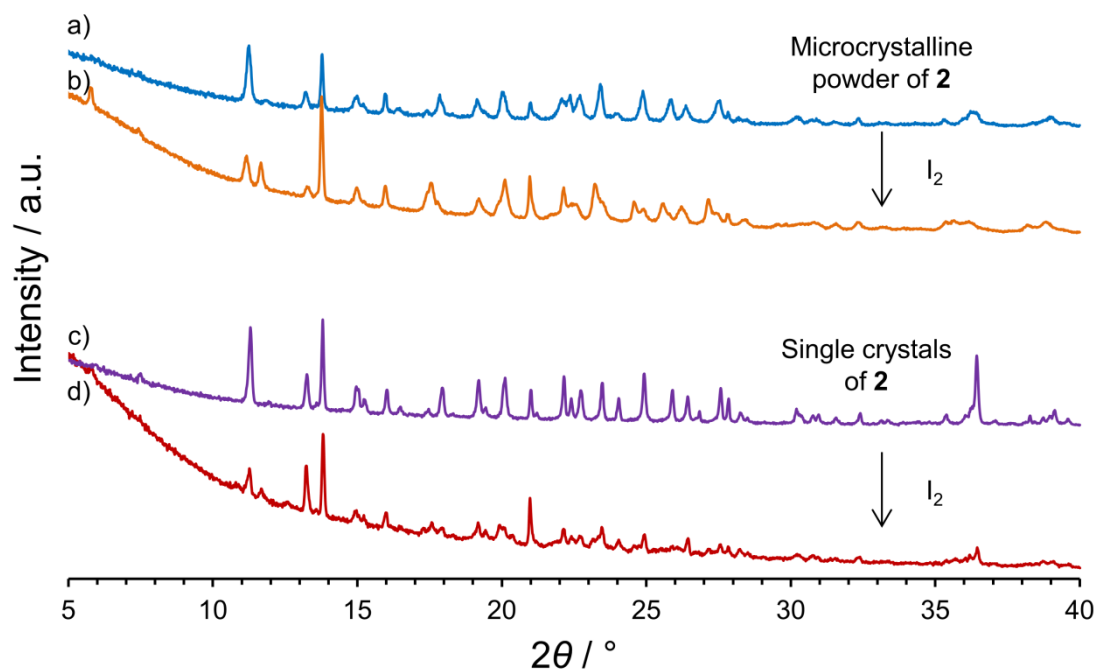


Fig S16. Overlay plot of the observed XRPD patterns of I₂ encapsulation in microcrystalline powder and single crystals of **2**. a) Microcrystalline powder of **2**. b) Microcrystalline powder of **2** after exposure to I₂ vapor for 12h. c) Single crystals of **2**. d) Single crystals of **2** after exposure to I₂ vapor for 12h.

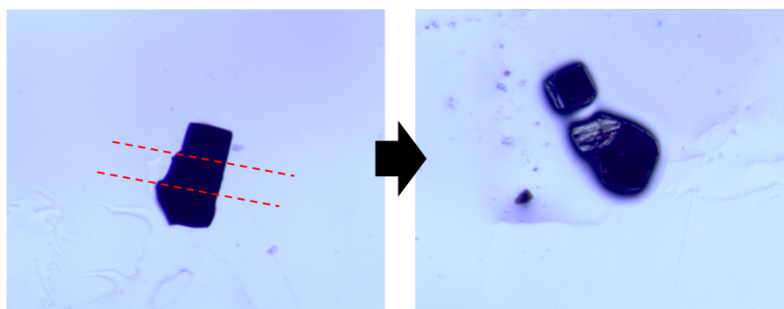


Fig S17. Microscope images of a single crystal of **2** after exposure to I₂ vapor for 12h without nitrobenzene treatment. Left) As it is after exposure to I₂ vapor, showing crystal surface was covered with I₂. Right) Cracked by a cutter at red broken lines and inverted, showing colorless inside.

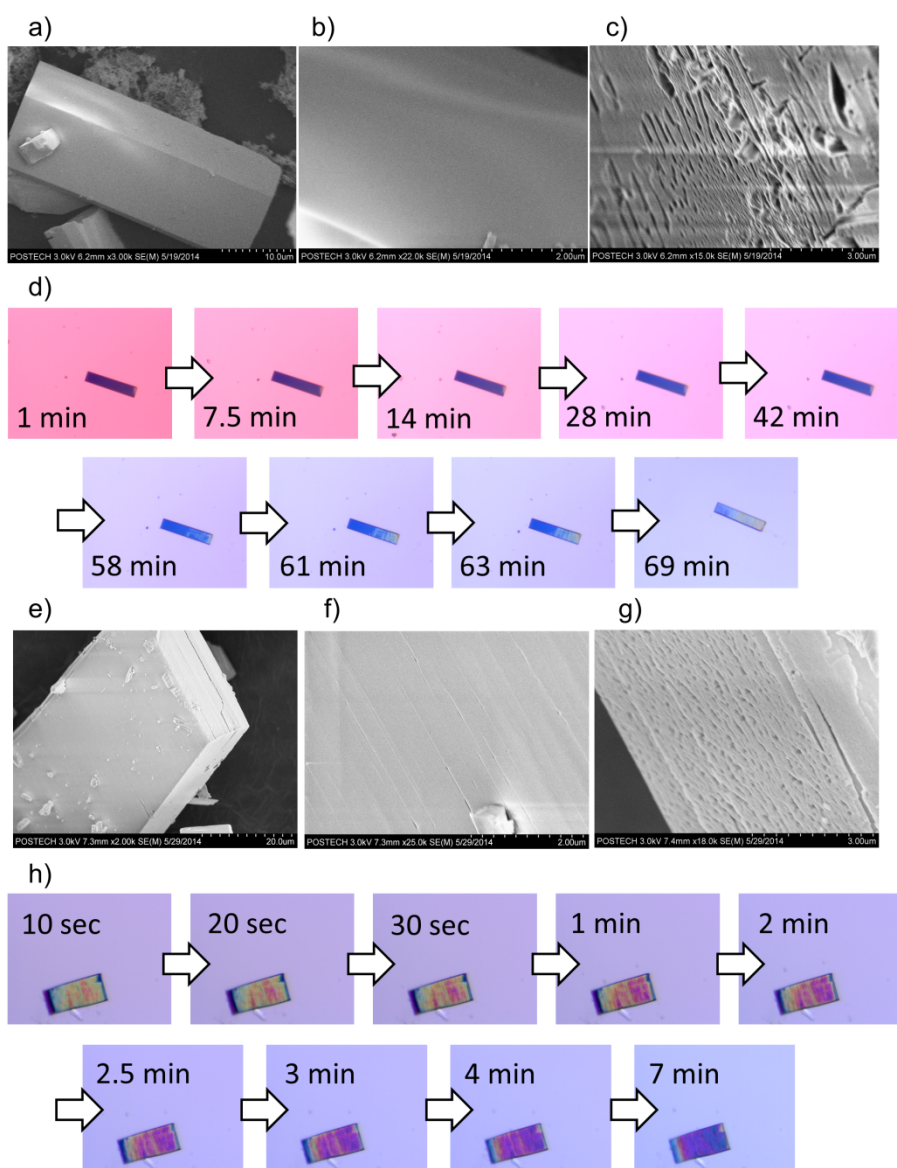


Fig S18. SEM images of **2** and microscope images of **2** immersed in I_2 nitrobenzene solution without and with nitrobenzene treatment. (a-b) SEM images of smooth *bc* and *ca* crystal surface of **2** without nitrobenzene treatment. c) SEM image of a rough *ab* crystal surface of **2**, indicating porous channels without nitrobenzene treatment. d) Microscope images of a single crystal of **2** immersed in I_2 -nitrobenzene solution under polarizer. Neither polarization nor surface of crystal changed for 42 min, and, after evaporation of I_2 , both of them changed from the cut edge. (e-f) SEM image of *bc* and *ca* crystal surface of **2** having many cracks with nitrobenzene treatment. g) SEM image of a rough *ab* crystal surface of **2**, indicating porous channels with nitrobenzene treatment. h) Microscope images of a single crystal of **2** with nitrobenzene treatment immersed in I_2 -nitrobenzene solution under polarizer. Polarization and surface of crystal changed uniformly just after immersing.

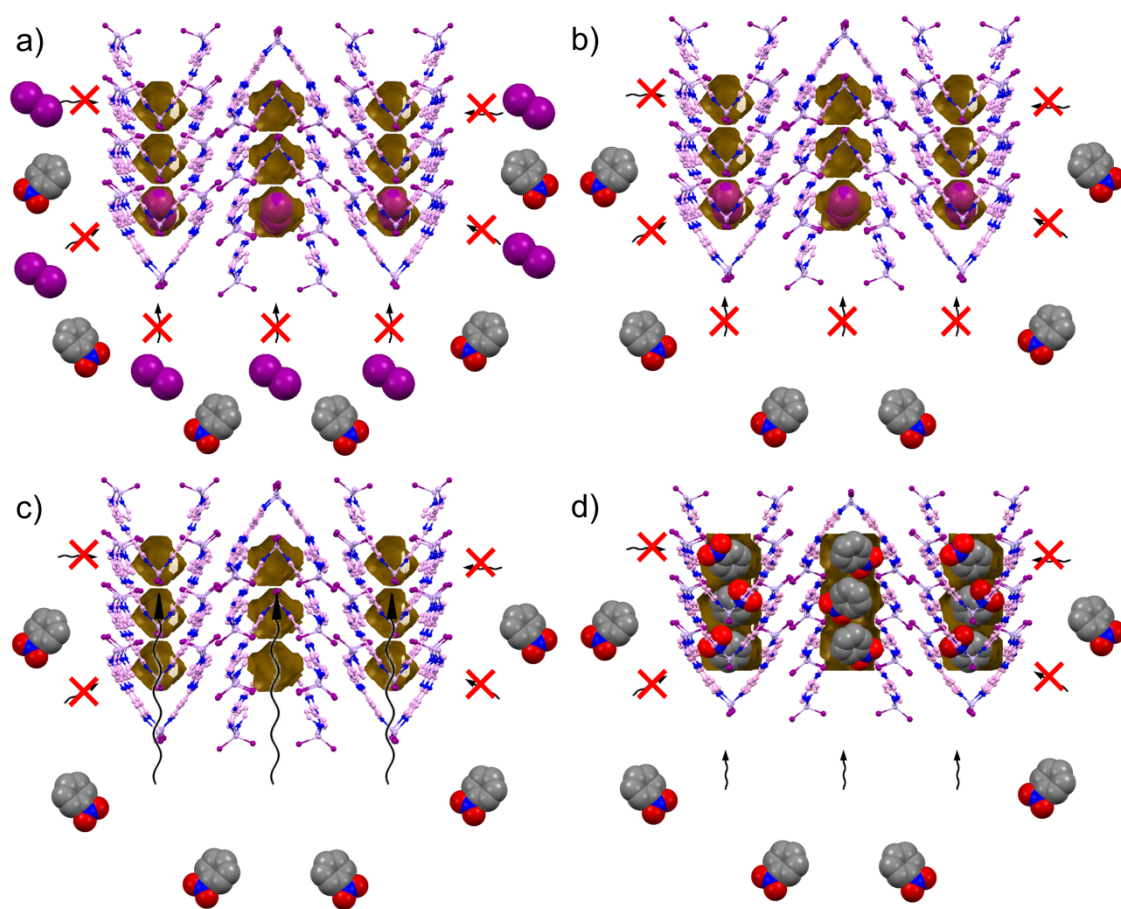


Fig S19. Scheme of capping the channel entrance by I_2 and nitrobenzene encapsulation. a) I_2 molecules block the entrance of 1D channel and subsequent I_2 molecules and nitrobenzene cannot go through the 1D channel (~42 min). b) Evaporation of I_2 from the solution (~58 min). c) Nitrobenzene molecules start encapsulating along the pore (~ 61 min). d) Nitrobenzene accommodation in the pores.

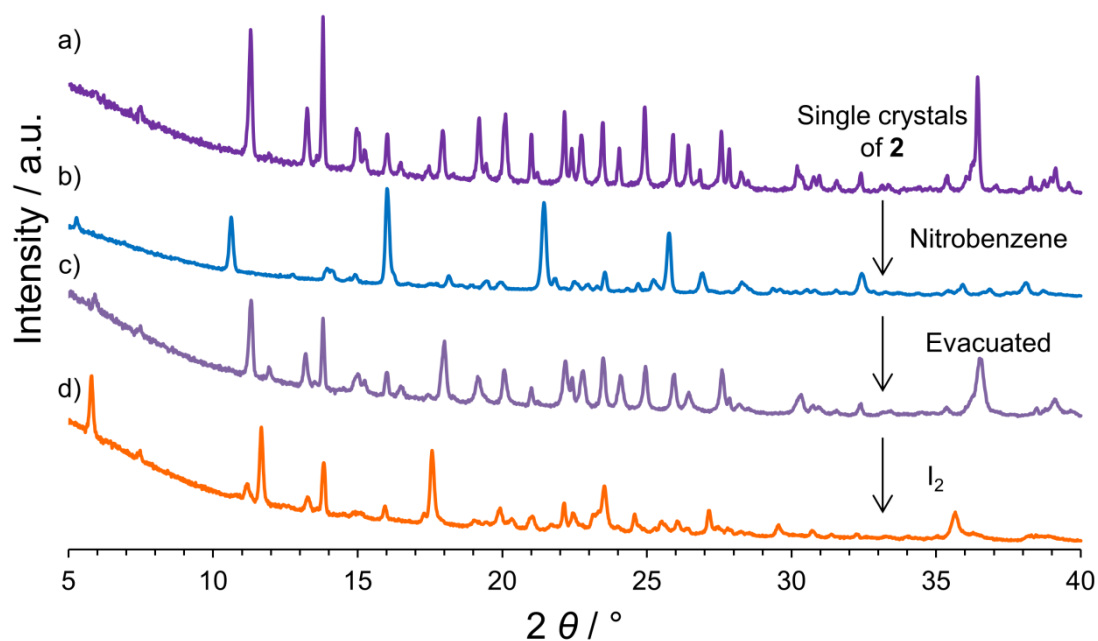


Fig S20. Overlay plot of the observed XRPD patterns of nitrobenzene treatment and I₂ encapsulation in single crystals of **2**. a) Single crystals of **2**. b) Single crystals of **2** after immersing in nitrobenzene. c) Single crystals of **2** after evacuating **2**-nitrobenzene for 6 hours at 200°C. d) Single crystals of **2** after exposure to I₂ vapor for 12h with nitrobenzene treatment.

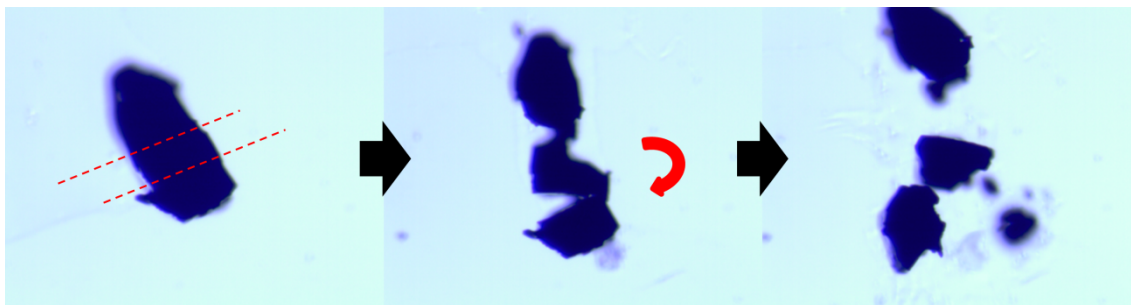


Fig S21. Microscope images of a single crystal of **2** with nitrobenzene treatment after exposure to I₂ vapor for 12h. Left) As it is after exposure to I₂ vapor, showing crystal surface was covered with I₂. Center) Cracked by a cutter at red broken lines. Right) Inverted, showing black inside.

References

- [1] L. H. Anderson, S. Anderson, M. K. Sanders, *J. Chem. Soc., Perkin Trans. I.* **1995**, 2231.
- [2] Z. Otwinowski, W. Minor, *Methods Enzymol.* **1997**, 276A, 307.
- [3] A. L. Spek, *PLATON, A Multipurpose Crystallographic Tool*; Utrecht University: Utrecht, The Netherlands, 1985.
- [4] G. M. Sheldrick, *Acta Crystallogr., Sect. A* **2008**, 64, 112.